Optical Design of PICO, a Concept for a Space Mission to Probe Inflation and Cosmic Origins

Karl Young[a], Marcelo Alvarez[b], Nicholas Battaglia[c], Jamie Bock[d], Jullian Borrill[e], David Chuss[f], Brendan Crill[g], Jacques Delabrouille[h], Mark Devlin[i], Laura Fissel[j], Raphael Flauger[k], Daniel Green[l], Kris Gorksi[g], Shaul Hanany[a], Richard Hills[m], Johannes Hubmayr[n], Bradley Johnson[o], Bill Jones[c], Lloyd Knox[p], Al Kogut[q], Charles Lawrence[g], Tomotake Matsumura[r], Jim McGuire[g], Jeff McMahon[s], Roger O'Brient[g], Clem Pryke[a], Xin Zhi Tan[a], Amy Trangsrud[g], Qi Wen[a], and Gianfranco de Zotti[t]

[a]University of Minnesota, USA
[b]University of California Berkeley, USA
[d]California Institute of Technology, USA
[e]Lawrence Berkeley National Laboratory, USA
[f]Villanova University, USA
[g]Jet Propulsion Laboratory, California Institute of Technology, USA
[h]Laboratoire AstroParticule et Cosmologie adn CEA/DAP, France
[i]University of Pennsylvania, USA
[j]NRAO, USA
[k]University of California, USA
[l]University of Toronto, Canada
[m]Cavendish Laboratory, University of Cambridge, UK
[n]NIST, USA
[o]Columbia University, USA
[c]Princeton University, USA
[p]University of California Davis, USA
[q]Goddard Space Flight Center, USA
[r]Kalvi IPMU, University of Tokyo, Japan
[s]University of Michigan, USA
[t]Osservatorio Astronomico di Padova, Italy

ABSTRACT

Abstract Submitted Nov. 2017, needs polishing.

The Probe of Inflation and Cosmic Origins (PICO) is a probe-class mission concept currently under study by NASA. PICO will probe the physics of the Big Bang and the energy scale of inflation, constrain the sum of neutrino masses, measure the growth of structure in the universe, and constrain its reionization history by making full sky maps of the cosmic microwave background with sensitivity 70 times higher than the Planck space mission. With broad frequency coverage from a few tens to hundreds of GHz, PICO will make polarization maps of galactic synchrotron and dust emission, thus elucidating the role of galactic magnetic fields in the process of star formation.

To be added Further author information: (Send correspondence to A.A.A.)
A.A.A.: E-mail: aaa@tbk2.edu, Telephone: 1 505 123 1234
B.B.A.: E-mail: bba@cmp.com, Telephone: +33 (0)1 98 76 54 32

We describe the PICO instrument, including the 1.4 meter telescope, the frequency coverage, the detector technology, and the intended survey of the sky. We will discuss the choice of optical system, present the design of the focal plane, and give the expected noise level.

Keywords: Cosmic microwave background, cosmology, mm-wave optics, polarimetry, instrument design, satellite, mission concept

1. INTRODUCTION

Probe study language copied directly from Brian's paper (May 6th). What level of repeat is useful and what is appropriate?

In astronomy and astrophysics, NASA currently flies small and medium Explorer missions (<$250M), as well as multi-billion-dollar flagship observatories like JWST and WFIRST. There are a number of science opportunities that are beyond the scope of the Explorer program, but don't require flagship-level funding. To explore these opportunities, NASA has funded studies of 10 'Probe' class ($400M-$1B) mission concepts. The Probe of Inflation and Cosmic Origins (PICO) is one of these mission studies. Reports of these mission studies are due to NASA at the end of the 2018 and NASA's plan is to forward the reports for consideration by the next Astronomy and Astrophysics Decadal panel. This paper comes part way through the PICO study, and describes a snapshot of the instrument design at this time in the study.

Brian's science section copied in .tex document. Repeating all of that here seems inappropriate. I have attempted to summarize. Mostly this is the first paragraph from Brian's paper.

Astrophysical observations in the millimeter and sub-millimeter region of the electromagnetic spectrum contain a wealth of information about the formation, evolution, and current structure of the Universe. Much of the large scale cosmological and fundamental physics information, such as evidence of inflation, the effect of the first stars and galaxies, constraints on neutrino masses, and limits on new light particles beyond the standard model, is contained in the temperature and polarization anisotropies of the cosmic microwave background (CMB). Information about the role of magnetic fields in star formation and galactic evolution is obtainable by observing the polarized emission of Galactic dust, which traces magnetic fields, at high resolution. Targeting both of these regimes, PICO will survey the entire sky with unprecedented polarization sensitivity in 21 bands centered at 21–799 GHz. Details of these science targets and expected constraints from PICO are in a companion paper, Ref. 1. In this paper we discuss the optical system, focal plane, and expected sensitivity of PICO.

2. SPACECRAFT AND MISSION

The PICO mission plan is to conduct scientific observations for five years from the Earth-Sun L2 Lagrange point. The spacecraft design impacts the optical design and sensitivity in two primary ways; volume constraints limit the physical size of the telescope and optical component temperatures impact noise levels. We discuss these major drivers here, other details are given in Ref. 1.

The maximum size of the spacecraft is limited by the assumed launch vehicle, the Falcon 9, which carries payloads up to 4.6 m in diameter. This diameter limit sets the V-groove size which, along with the scan strategy, defines the 'shadow cone' in Figure 1. The shadow cone is the volume which is never illuminated by the sun and all optical components must remain within it. The shadow cone and inner V-grooves define an available volume for the telescope which is.

The temperatures of all optical elements are given in Figure 1. The primary is passively cools to 40 K, as was seen for *Planck*.[2] The secondary, optics box, and aperture stop are actively cooled to 6 K. The focal plane is cooled by a continuous ADR to 100 mK.

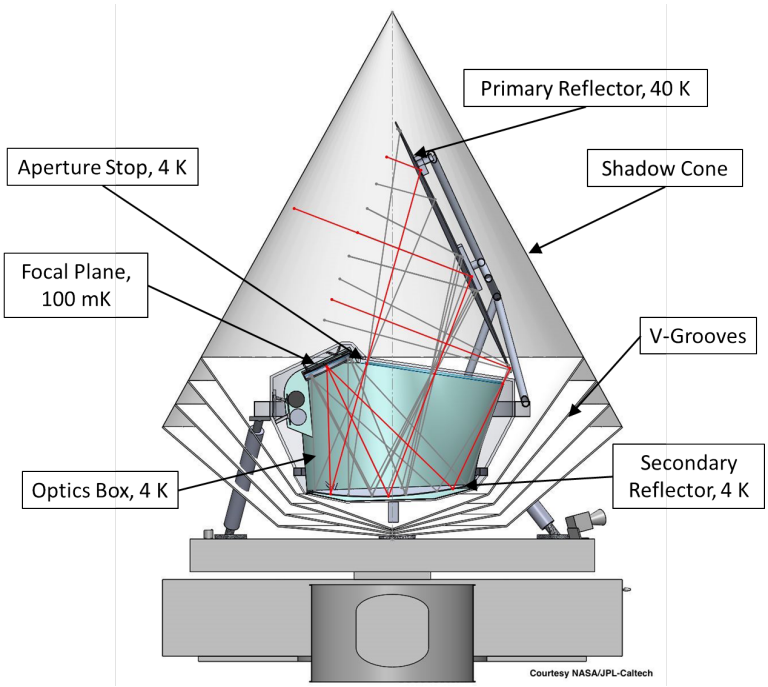

Figure 1. Mechanical design of the PICO satellite. Components relevant to this paper are labeled, for other details see Ref. 1. Update temperatures with final numbers from JPL

3. OPTICAL SYSTEM

The PICO telescope is a 1.4 m modified Open Dragone. This choice was driven by a combination of science requirements and the physical limits discussed in Section 2. The science requirements are; a large diffraction limited field of view (DLFOV) sufficient to support $\mathcal{O}(10^4)$ detectors, arcminute resolution at 799 GHz, low instrumental polarization, and low sidelobe response. Additionally, the transition edge sensor bolometers baselined for PICO require a telecentric focal plane which is sufficiently flat that it can be tiled by 10 cm detector wafers without reduction in optical quality. These requirements suggest an off-axis Dragone system[3] similar to what has been used for *Planck*,[4] various ground based systems such as ACT[5] and SPT,[6] and in the CORE[7] and LiteBIRD[8] designs.

The geometric parameters of the PICO optical system are given in Table 1 and the ray trace in Figure 2. The system is diffraction limited, Strehl greater than 0.8, at the center of the field of view for 799 GHz and has a DLFOV of 82.4 deg^2 at 155 GHz. Strehl of 0.8 contours for all pixel types are shown in Figure 2. The slightly concave, 4.55 m radius of curvature, focal plane is telecentric to within 0.12 deg across the entire surface.

To arrive at the final design we modify an Open Dragone. We follow Ref. 9 to design the initial Open Dragone. We find a solution which satisfies the volume constraints and has a large DLFOV. We force a circular aperture stop between the primary and secondary mirrors and numerically optimized its angle and position to obtain the best optical performance. The stop diameter was chosen to provide an effective 1.4 m aperture on the primary for the center feed. Adding a stop in this way increases the size of the primary mirror, effectively the primary is unevenly illuminated at various field angles, but reduces detector noise, see Section 5, and helps control sidelobes. At this stage the system still meets the Dragone condition and is defined by the 'Initial Open Dragone' parameters in Table 1.

To increase the optical performance we use CodeV to numerically optimize the system. To adjust the mirror shapes, we add a low order, 4th and 9th-13th, Zernike polynomial correction to each conic surface. We allow focal plane curvature, a focal plane tilt angle, and the focal plane to secondary distance to vary. The primary-secondary distance, primary offset h, and the primary and secondary rotation angles, α and β, are varied as

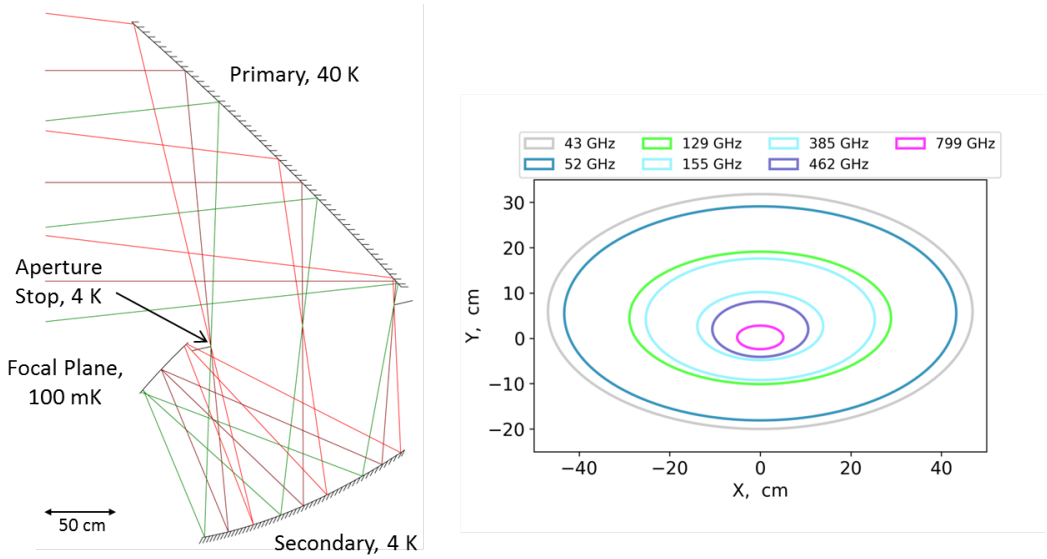

Figure 2. Raytrace (left) and Strehl = 0.8 contours (right) for the PICO optical design. strehl needs a legend to give frequencies

Table 1. Telescope parameters needs cleaning and some more numbers looked up. Are Zernike coefficients even useful?

PICO optical system					Initial Open Dragone	
	Primary	Secondary	Telescope parameters		Fundamental design parameters	
Size (cm)	268 × 206 ?check?	160 × 158 ?check?	Aperture (m)	1.4	Aperture (m)	1.4
Radius of curvature (cm)	∞	136.6	Focal ratio, F	1.42	θ_0 (degrees)	90
Conic constant, k	0	-0.926	h (cm)	430?	θ_e (degrees)	20
Normalization radius	524.8	194.1	α	?	θ_p (degrees)	140
4th Zernike Coefficient	2018.4	-61.1	β	?	L (cm)	240
9th Zernike Coefficient	-37.0	16.7	L	?	Derivative parameters	
10th Zernike Coefficient	-2919.8	-15.1	d_{SR-FP}	?	Focal ratio, F	1.42
11th Zernike Coefficient	-1292.7	22.3			h (cm)	624.2
12th Zernike Coefficient	120.6	-3.8	Focal Plane		α	38.6
13th Zernike Coefficient	-74.5	4.9	FP diameter (cm)	69 x 45	β	101.4
19th Zernike Coefficient	-75.8	3.4	FP diamter (deg)	19 x 13	Primary, f (cm)	312.1
20th Zernike Coefficient	-398.9	6.3	FP tilt (deg)	?check?	Secondary, e	1.802
21st Zernike Coefficient	-319.5	23.3			Secondary, a (cm)	131
22nd Zernike Coefficient	-276.6	-8.5				
23rd Zernike Coefficient	-201.6	-3.2				
24th Zernike Coefficient	-127.4	-1.9				
25th Zernike Coefficient	-55.0	0.1				

need some explanatory footnotes.

well. The optimization metric is the rms spot size across the field of view, with additional weighted constraints requiring telecentricity and maintaining the x- and y-focal lengths. We also added Lagrange constraints to enforce beam clearences and put an upper limit on overall system size. Once the optimization coveraged to an acceptable optical system, we added the higher order Zernike terms, 19th-25th, and refined the mirror shapes using the same metric and constraints.

In Figure 3 we show the final optimized system compared with the 'Initial Open Dragone' and give the Strehl = 0.8 contours. One sees the optimization reduced the overall telescope volume, allowing it to fit more easily within the shadow cone and increased the DLFOV. The most important increase in the DLFOV is at 155 and 186 GHz. This added area allows us to add 'C' and 'D' pixels which are the main CMB workhorses and drive PICO's sensitivity. Being able to pack 100's of these pixels into the focal plane is what allows PICO to reach unprecedented levels of sensitivity.

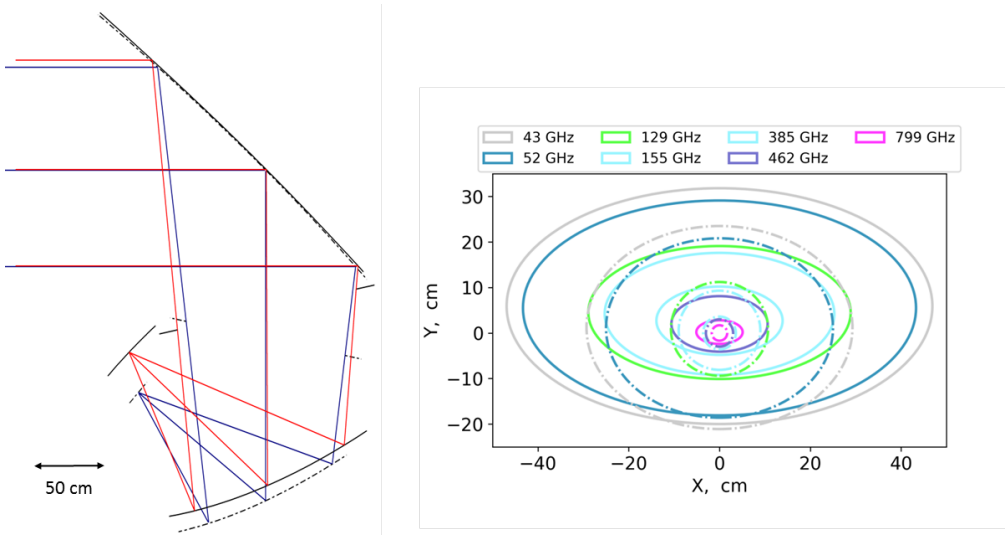

Figure 3. Comparison between optimized and unoptimized Open Dragones. The raytraces (left) are aligned at the chief ray impact point on the primary. The optimized system (red rays, solid mirrors) is smaller vertically and has a slightly flatter primary than the unoptimized version (blue rays, dash-dot mirrors)need to change mirror lines. The overlaid Strehl = 0.8 contours (right) show the improvement at all frequencies in the optimized (solid lines) over the unoptimized (dash-dot lines) system. strehl needs a legend to give frequencies

An additional benefit of the optimization is the concave focal plane. The Open Dragone's focal surface is naturally curved, so matching this curvature reduces defocus and increases the DLFOV as well as increasing telecentricity. The unoptimized system is telecentric to within 2.5°while the optimized version is telecentric to within 0.12°.

We considered two additional Dragone systems; a Gregorian Dragone like that used for *Planck* and a Crossed Dragone similar to that planned for CORE or LiteBIRD. The Gregorian Dragone has insufficient DLFOV,[7] roughly 3× less in area for a similar system, so was rejected. The Crossed Dragone has an intrinsically larger DLFOV than the Open, but it has well known issues with sidelobes as shown in Figure 4 and always has a larger F-number than the Open system. The larger F-number results in a larger telescope that fits poorly into the shadow cone. The largest Crossed Dragone that meets the PICO volumen contraints has a 1.2 m aperture while a 1.4 m Open Dragone fits. The large F-number of the Crossed system also increases the physical focal plane size, and therefore mass and cost, for a fixed number of pixels. These disadvantages and the success of the optimized Open Dragone led us to the final PICO optical system detailed in Table 1 and shown in Figure 2.

4. FOCAL PLANE

Modern mm/sub-mm detectors are photon noise limited, so the primary way to increase sensitivity is to increase the number of detectors on sky. The PICO focal plane has 12,996 detectors, a factor of 175 more than *Planck*. PICO achieves this by having a large DLFOV and using multichroic pixels (MCP).[10] Multichroic pixels are a recent mm-wave pixel technology made up of a broad-bandwidth polarization sensitive antenna lithographed onto a silicon substrate which couples to microstrip transmission lines to carry the signal to a channelizing filter. The filter divides the broadband signal into individual bands and directs it to separate transition edge sensor (TES) bolometers. The architecture assumed for PICO uses three bands per pixel; each pixel contains two single polarization bolometers per band and therefore six bolometers total. Using MCP increases the number of bolometers by a factor of six without increasing the required focal plane area.

We designed PICO with 21 overlapping bands centered at 21–799 GHz and divided amongst nine pixel types, A-I, shown in Figure 5, These bands provide the broad fequency coverage needed to seperate the CMB, Galactic dust, and various foreground using their differing spectra. The PICO bands are logarithmically spaced with 25% fractional bandwidth. The bandwidth is broader than the interband spacing meaning the bands overlap and

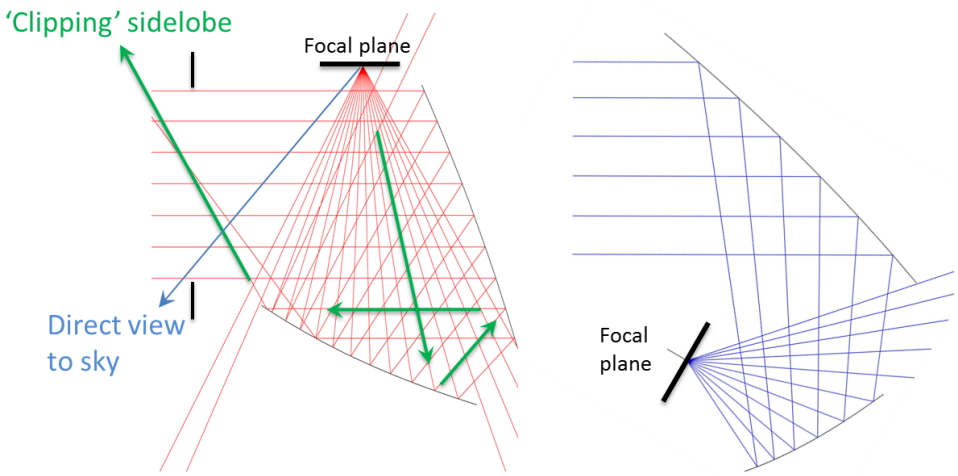

Figure 4. Comparison of sidelobes for example Crossed (left) and Open (right) Dragones. Rays are traced from the center of the focal plane toward the sky. For both systems spillover around the secondary is straightforward to mitigate with absorptive baffles. However, the clipping sidelobe and direct sky view in the Crossed system require a long forebaffle or large F-number to mitigate, both of which were problematic in the PICO case.

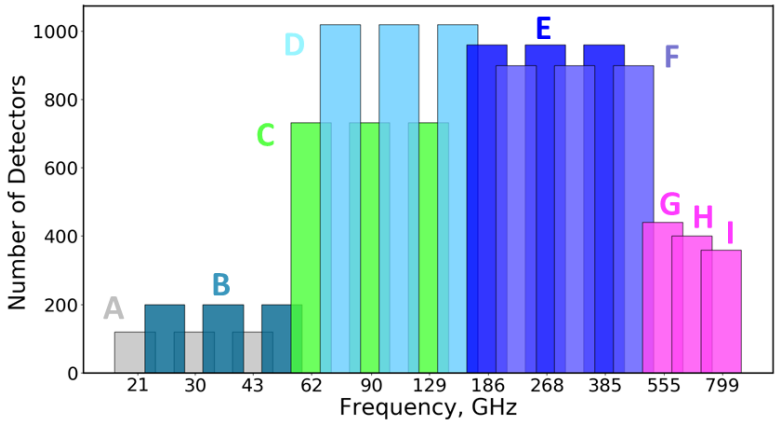

Figure 5. Frequency coverage of the PICO bands. Each color (except magenta) denotes a different MCP, labeled A-F. The bar height indicates the number of detectors per band. Width gives the bandwidth, all are top-hats with 25% fractional bandwidth; the x-axis is logarithmic. The three highest frequencies (magenta) are single color pixels G, H, I. Confusion likely because 'E' is blue in this plot, but cyan in the focal plane. Need to address this.

neighboring bands must be in separate pixels. For example, bands 1, 3, and 5 are in pixel A while bands 2, 4, and 6 are in pixel B. This complicates the pixel design and focal plane layout, but allows broader brands to increase total sensitivity. The exceptions to this MCP architecture are the highest three bands. These three bands are single frequency, because they are above the superconducting band gap of niobium meaning the standard niobium transmission lines and filters cannot be used. Instead we will use absorber coupled bolometers at these frequencies.

The PICO focal plane is designed to take maximum advantage of the large field of view. As discussed in Section 3, the optical quality peaks at the focal plane center and falls off with radius. This pattern dictates the layout shown in Figure 6, with the highest frequency pixels centered in the focal plane and low frequency pixels around the edge. The maximum radial distance for a given pixel is the point where the Strehl ratio for the highest frequency band within that pixel equals 0.8. Interior to these contours, the ellipses in Figure 6, the

Strehl ratio increases ensuring pixels are diffraction limited.

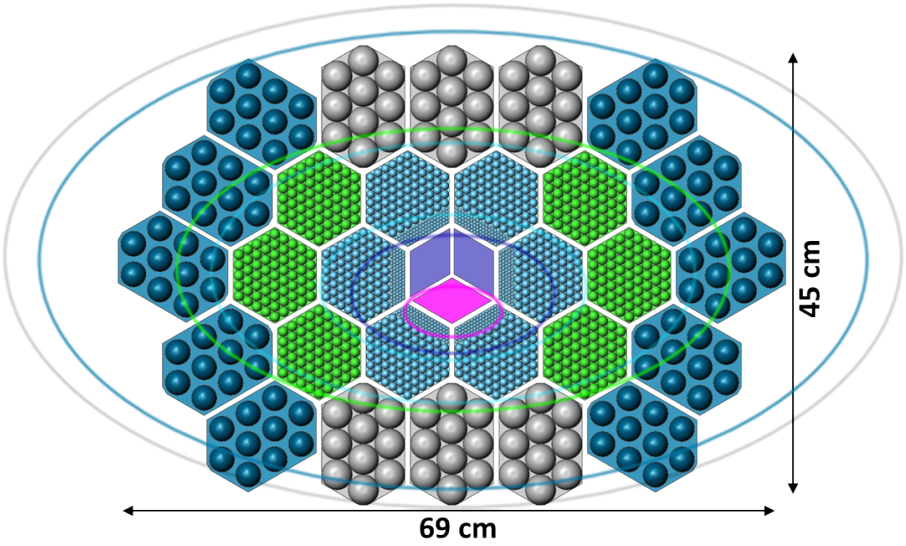

Figure 6. PICO focal plane layout with Strehl = 0.8 contours for each pixel type. The pixel and Strehl contour colors match the band colors, A-I, in Figure 5 Strehls make in more visible format, certainly cyan contours.

Optimizing the pixel size is a balance between number of pixels and the efficiency with which they couple to the telescope. Smaller pixels pack more densely on the focal plane, number scaling as $1/D_{px}^2$, but over illuminate the stop which reduces total efficiency and adds thermal load. We choose a pixel spacing of $2.1F\lambda$, giving an edge taper on the stop of 10 dB, for the center band of each pixel. Due to the multichroic nature of the pixels this edge taper varies with band, details in Section 5. We hex-pack pixels onto 94 mm hexagonal wafers to minimize wasted space for the mid-frequency pixels. The three central wafers have the same 94 mm hexagon footprint but are split into 3 rhombi as seen in Figure 6, because the highest frequency magenta wafer will use different detector technology and will need to be fabricated separately. Laying out the focal plane we assume lenslets[10] will be used to couple the antennas to free space, but the exact coupling scheme has not been finalized. However, the pixel size, number, and spacing is relatively agnostic to the coupling scheme, so we do not expect significant changes to the current layout even if horn or phased array coupling is used in the final design.

Discuss Q/U orientation?

Reading out 12,996 TES bolometers requires significant multiplexing. Time domain (TDM) and frequency domain (FDM) multiplexing were explored for PICO, tradeoff details are in Ref. 1. The current PICO baseline is TDM, but the choice is not a driver for the focal plane layout or noise discussed in this paper.

5. NOISE MODEL

comment somewhere in this section that these noise numbers are CBE. no margins.

We developed an end to end white noise only model of the PICO instrument to predict full mission sensitivity and provide a metric by which to evaluate optical, mechanical, and mission design tradeoffs. To simplify the model, we assume TES bolometers as the detector at all frequencies, even though other technologies may be better suited to the lowest bands. Any suitable technology will be photon noise dominated as the TESs are, so total noise levels in the lowest bands should be relatively unaffected by the use of a different detector technology. We constructed the model following the methods in Ref. 11 and 12; estimate the optical load, calculate properties of the TES bolometers, calculate noise equivalent power (NEP) for each source, combine all NEP terms to get detector noise, and finally calculate full mission sensitivity. Each of these steps includes various assumptions and design decisions, which are discussed in this section. The assumptions are summarized in Table 2.

Table 2. Noise model assumptions, see text for details. listing still in flux

Throughput	single moded, λ^2
Fractional Bandwidth	25%
Mirror emissivity	$\epsilon = \epsilon_0\sqrt{\nu/150\ \mathrm{GHz}}, \epsilon_0 = 0.07\%$
Aperture stop emissivity	1
Low pass filter reflection loss	8%
Low pass filter absorption loss	frequency dependent, $\approx 2\%$ change to appropriate range
Bolometer absorption efficiency	70%
T_e for middle band in pixel (dB)	10
Mission length (years)	5
Observing efficiency	95%
Safety factor, P_{sat}/P_{abs}	2
Bose noise fraction, ξ	1
T_o (mK)	100
T_c (mK)	187
Thermal power law index, n	2
SQUID noise (aW/$\sqrt{\mathrm{Hz}}$)	3.5 (FDM), ?? (TDM)
TES operating resistance, ohm	1 (FDM), 0.03 (TDM)
TES transition slope, alpha	100 (TDM)
TES loop gain	25 (FDM), 14 (TDM)
other?	
footnote to explain LP filter absorption	

5.1 Single bolometer noise

The sources of optical load are the CMB, primary and secondary mirrors, the aperture stop, and a low pass optical filter. These elements are shown schematically in Figure 7. We assume the primary is 40 K, the stop and secondary 4 K, and the low pass filter 100 mK. The emissivity of the mirrors depends on frequency, $\epsilon(\nu) = \epsilon_0\sqrt{\nu/(150\ \mathrm{GHz})}$. At 150 GHz we assume an emissivity of 0.07%.[2,13]

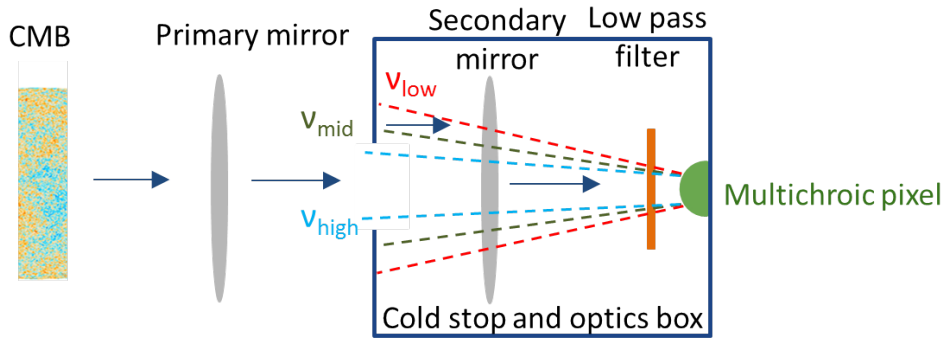

Figure 7. Schematic representation of the prediction of optical load. Power emitted by each element is modified by the efficiency of the following elements and added to the total expected load. The multichroic pixel illuminates the stop differently for each of the three bands.

The total load absorbed at the bolometer is the sum of the power emitted by each element reduced by the optical efficiency of the elements between the emitting surface and the bolometer. For example, the CMB power is reduced by the optical efficiency of the entire instrument, $\eta_{opt} = \eta_{PRI}\eta_{stop}\eta_{SEC}\eta_{filter}\eta_{bolo}$, while the power emitted by the low pass filter is reduced only by η_{bolo}. The absorbed power is,

$$P_{abs} = ((((P_{CMB}\eta_{PRI} + P_{PRI})\eta_{stop} + P_{stop}(1-\eta_{stop}))\eta_{SEC} + P_{SEC})\eta_{filter} + P_{filter})\eta_{bolo}, \quad (1)$$

where P_{elem} is the in band power emitted by a given element for a single polarization and η_{elem} is the efficiency of the element. We assumed 25% fractional bandwidth top-hat bands and throughput of λ^2. Power from the stop is a special case. We multiply P_{stop} by $(1-\eta_{stop})$ because η_{stop} is spillover efficiency, the fraction of the throughput which passes through the stop, so $(1-\eta_{stop})$ is the fraction of the throughput which views the stop.

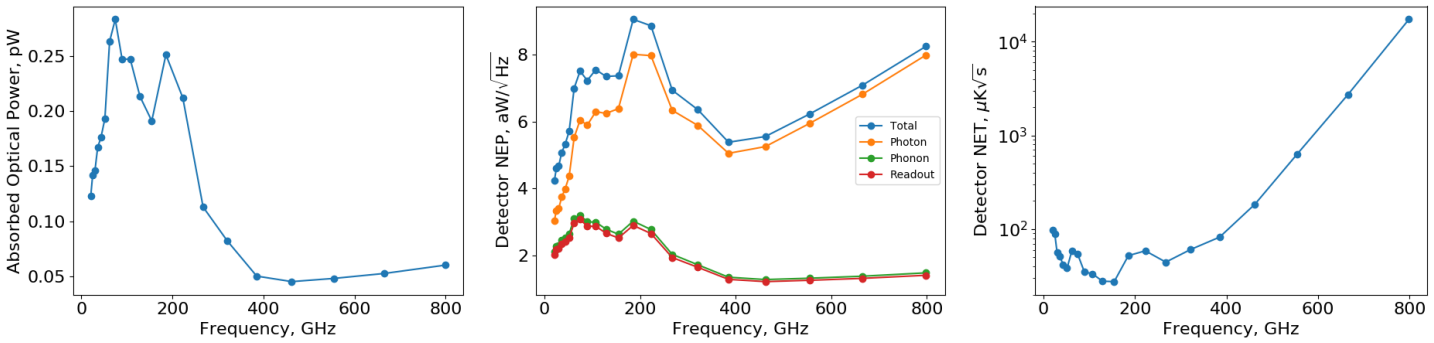

Figure 8. Left: Expected optical loads for single polarization PICO bolometers. Center: Breakdown of NEP across the PICO frequency range. Photon noise dominates even at the lowest frequencies. Right: Per detector NET, temperature sensitivity, across the PICO bands. could add CORE NETs here for comparison. could add zoom around 150 GHz.

For PICO, the CMB and stop are the major load at low frequencies while and mirror emission is the majority above 460 GHz due to their differing temperatures, see Figure 8. The jumps in load between neighboring bands in Figure 8, around 70 and 200 GHz are due to η_{stop} changing with frequency. This is driven by the use of multichroic pixels whose angular beam pattern is dependent on the pixel diameter,[11]

$$\theta_{1/e^2} = \frac{2.95\lambda}{\pi D_{px}}. \tag{2}$$

The edge taper, T_e, of the middle frequency band in each pixel is chosen to be 10 dB. For the upper and lower bands T_e is calculated using Equation 2. This changing illumination of the stop is shown schematically by the dashed rays in Figure 7. For each MCP, A-H, T_e is 4.8, 10, and 20.7 dB for the lower, middle, and upper bands, respectively. These edge tapers correspond to η_{stop} of 0.68, 0.90, and 0.99. The changing η_{stop} has thee main effects; uneven optical load between bands, varying NEP to noise equivalent temperture (NET) conversion between bands, and telescope beam size not scaling smoothly with λ.

From P_{abs} we calculate the TES bolometer properties for each band. We assume a safety factor of 2, $P_{sat}/P_{abs} = 2$; P_{sat} is the saturation power of the bolometer. The PICO focal plane temperature, T_o, of 100 mK sets an optimal superconducting transition temperature, T_c, of 187 mK. We assume thermal conductivity scales as a power law, $G \propto T^n$, with $n = 2$. The required thermal conductivity for a given bolometer is set by the P_{sat},

$$G = \frac{P_{sat}}{T_c}(n+1)\frac{1}{1-(T_o T_c)^{n+1}}. \tag{3}$$

We consider three noise sources per bolometer; photon, phonon, and readout. Photon noise depends on the absorbed power,[14]

$$NEP_\gamma^2 = \int_{band} 2h\nu p\, d\nu + 2\xi \int_{band} p^2 d\nu, \tag{4}$$

where p is the power spectral density for a single polarization absorbed at the bolometer and ξ is the fraction of correlated Bose photon noise. We assume $\xi = 1$. For PICO, $\mathrm{NEP}_{Bose}/\mathrm{NEP}_{Poisson} = 1.3$ in the lowest band but since Bose noise does not scale with $\sqrt{\nu}$ as Poisson does $\mathrm{NEP}_{Bose}/\mathrm{NEP}_{Poisson} < 10\%$ at 268 GHz.check if this is NEP/NEP or NEP^2 The second largest noise term is phonon noise[15] in the thermal connection to T_o,

$$NEP_{phonon}^2 = 4\gamma k_b T_c^2 G, \tag{5}$$

where γ is a unitless factor depending on T_o, T_c, and n. For PICO $\gamma = 0.5$. Readout noise depends on the assumption of FDM or TDM readout and includes all remaining noise sources, the Johnson noise of the TES as well as all components not intrinsic to the bolometers. For both multiplexing schemes $\mathrm{NEP}_{readout}$ is dominated by the SQUID amplifier with moderate contributions from various resistors and amplifiers in the readout chain. We calculate noise for both FDM and TDM systems, though TDM is the current baseline, and find both to be below both photon and phonon noise for all bands. Both systems give similar noise levels, with total noise differing by less than 3% in all bands. Some thought has been put into optimizing the readout systems for space, but since the expected noise is already sufficiently low this was not pursued in detail. For TDM and FDM the noise primarily scales with TES bias voltage which depends on the electrical power needed to operate the TES,

$$\begin{aligned} NEP^2_{readout} \propto V^2_{bias} \propto P_e, \text{ and} \\ P_e = P_{sat} - P_{abs}. \end{aligned} \tag{6}$$

This neglects the details of our readout noise models, but is an illustrative approximation usefull for this paper.

The noise breakdown in Figure 8 drives various aspects of the PICO design. Since photon noise dominates at all frequencies and photon noise scales with $\sqrt{P_{abs}}$, Equation 4, the primary driver of noise is optical load. The second largest source of noise is phonon noise. Combining Equations 3 and 5 we see NEP_{phonon} scales with $\sqrt{T_C}$ and $\sqrt{P_{sat}}$. Cooling the focal plane to 100 mK reduces T_c since $T_c \propto T_o$. The saturation power depends on the choice of safety factor, P_{sat}/P_{abs}, as well as on optical load. We choose safety factor of two to lower noise, while providing margin for unexpected loads or variations in G of the fabricated bolometers. Readout noise scales with $\sqrt{P_{sat} - P_{abs}}$, Equation 6, which is reduced by reducing the safety factor or P_{abs}. From this analysis we see that all noise sources depend on P_{abs}, either directly or through how load drives bolometer properties. Therefore the most straightforward way to reduce noise is to limit all optical loads other than the CMB. This motivates the simple, few element telescope we have designed with the aperture stop and secondary mirror actively cooled to reduce excess load and photon noise.

5.2 Combined array noise

Using single detector NEPs as per Section 5.1 and the detector counts from Section 4 we calculate the combined NEP of the detector array for each band. Generally, combining detectors simply reduces noise by $\sqrt{N}$. The one exception is Bose photon noise. For the lowest band of each MCP the pixels oversample the PSF, pixel spacing is 0.4Fλ, resulting in correlated Bose noise bewteen pixels. Accounting for this effect gives a XX% increase in the combined array NEP of the lowest band, 21 GHz, and only a XX% increase in the highest band, 799 GHz.

From the array NEP we convert to NET per band,

$$NET = \frac{NEP}{\sqrt{2}\eta_{opt} \int\limits_{band} \frac{dP}{dT}\Big|_{T_{CMB}} d\nu}. \tag{7}$$

The η_{opt} term contributes to the 'jumps' in NET seen in Figure 8 since η_{opt} varies band to band. We use CMB temperature units for all bands, even though this isn't particularly suitable for the highest bands, because the CMB is the most stringent requirement on sensitivity.

All the above calculations have been for sensitivity to temperature and are given in Table 3. Assuming evenly weighted observations of the full sky and 5 years observing at 95% efficiency we calculate full mission map sensitivities in polarization; final column in Table 3. Combining all bands gives a total CMB map depth for the entire PICO mission of 0.67 $\mu\mathrm{K}_{CMB}$-arcmin.

6. CONCLUSIONS/SUMMARY

- Total full sky map sensitivity, compare to Planck, LB, and S4? or do so in intro?

simple telescope. low noise? low systematics? - systematics not discussed elsewhere (yet)

Table 3. PICO frequency channels and noise. this assumes 4K, 40K, filter. may need to change

Pixel Type	Band GHz	FWHM arcmin	Bolometer NEP aW/$\sqrt{Hz}$	Bolometer NET $\mu K_{CMB}\sqrt{s}$	N_{bolo}	Array NET $\mu K_{CMB}\sqrt{s}$	Polarization map depth μK_{CMB}-arcmin
A	21	38.4	4.23	97.0	120	10.88	15.32
B	25	32.0	4.60	88.8	200	7.64	10.75
A	30	28.3	4.67	56.4	120	5.30	7.46
B	36	23.6	5.07	51.6	200	3.75	5.27
A	43	22.2	5.31	41.6	120	3.79	5.34
B	52	18.4	5.71	38.2	200	2.70	3.81
C	62	12.8	6.99	58.3	732	2.44	3.44
D	75	10.7	7.50	54.6	1020	1.90	2.67
C	90	9.5	7.22	35.0	732	1.31	1.84
D	108	7.9	7.54	33.3	1020	1.05	1.48
C	129	7.4	7.34	27.8	732	1.03	1.45
D	155	6.2	7.36	27.5	1020	0.86	1.21
E	186	4.3	9.04	52.1	960	1.72	2.43
F	223	3.6	8.85	58.6	900	1.99	2.80
E	268	3.2	6.93	44.4	960	1.43	2.02
F	321	2.6	6.35	60.3	900	2.01	2.83
E	385	2.5	5.38	82.1	960	2.65	3.73
F	462	2.1	5.55	184.1	900	6.14	8.64
G	555	1.5	6.22	632.3	440	30.15	42.44
H	666	1.3	7.08	2728.5	400	136.44	192.06
I	799	1.1	8.24	17297.3	360	911.70	1283.36
Total				12996	0.46	0.57	

7. ACKNOWLEDGEMENTS

This Probe mission concept study is funded by NASA grant xxxxxxxx.

REFERENCES

[1] Sutin, B. M., Alvarez, M., Battaglia, N., Bock, J., Bonato, M., Borrill, J., Chuss, D., Cooperrider, J., Crill, B., Delabrouille, J., Devlin, M., Fissel, L., Flauger, R., Gorski, K., Green, D., Hanany, S., Hubmayr, J., Johnson, B., Jones, W. C., Knox, L., Kogut, A., Lawrence, C., McMahon, J., Matsumura, T., Negrello, M., OBrient, R., Paine, C., Pryke, C., Trangsrud, A., Wen, Q., Young, K., and de Zotti, G., "Pico - the probe of inflation and cosmic origins," *Proc. SPIE* **10698** (2018).

[2] Planck Collaboration, Ade, P. A. R., Aghanim, N., Arnaud, M., Ashdown, M., Aumont, J., Baccigalupi, C., Baker, M., Balbi, A., Banday, A. J., Barreiro, R. B., Battaner, E., Benabed, K., Benoît, A., Bernard, J. P., Bersanelli, M., Bhandari, P., Bhatia, R., Bock, J. J., Bonaldi, A., Bond, J. R., Borders, J., Borrill, J., Bouchet, F. R., Bowman, B., Bradshaw, T., Bréelle, E., Bucher, M., Burigana, C., Butler, R. C., Cabella, P., Camus, P., Cantalupo, C. M., Cappellini, B., Cardoso, J. F., Catalano, A., Cayón, L., Challinor, A., Chamballu, A., Chambelland, J. P., Charra, J., Charra, M., Chiang, L. Y., Chiang, C., Christensen, P. R., Clements, D. L., Collaudin, B., Colombi, S., Couchot, F., Coulais, A., Crill, B. P., Crook, M., Cuttaia, F., Damasio, C., Danese, L., Davies, R. D., Davis, R. J., de Bernardis, P., de Gasperis, G., de Rosa, A., Delabrouille, J., Delouis, J. M., Désert, F. X., Dolag, K., Donzelli, S., Doré, O., Dörl, U., Douspis, M., Dupac, X., Efstathiou, G., Enßlin, T. A., Eriksen, H. K., Filliard, C., Finelli, F., Foley, S., Forni, O., Fosalba, P., Fourmond, J. J., Frailis, M., Franceschi, E., Galeotta, S., Ganga, K., Gavila, E., Giard, M., Giardino, G., Giraud-Héraud, Y., González-Nuevo, J., Górski, K. M., Gratton, S., Gregorio, A., Gruppuso, A., Guyot, G., Harrison, D., Helou, G., Henrot-Versillé, S., Hernández-Monteagudo, C., Herranz, D., Hildebrandt, S. R., Hivon, E., Hobson, M., Holmes, W. A., Hornstrup, A., Hovest, W., Hoyland, R. J., Huffenberger, K. M., Israelsson, U., Jaffe, A. H., Jones, W. C., Juvela, M., Keihänen, E., Keskitalo, R., Kisner, T. S., Kneissl, R., Knox, L., Kurki- Suonio, H., Lagache, G., Lamarre, J. M., Lami, P., Lasenby, A., Laureijs, R. J., Lavabre,

A., Lawrence, C. R., Leach, S., Lee, R., Leonardi, R., Leroy, C., Lilje, P. B., López-Caniego, M., Lubin, P. M., Macías-Pérez, J. F., Maciaszek, T., MacTavish, C. J., Maffei, B., Maino, D., Mandolesi, N., Mann, R., Maris, M., Martínez-González, E., Masi, S., Matarrese, S., Matthai, F., Mazzotta, P., McGehee, P., Meinhold, P. R., Melchiorri, A., Melot, F., Mendes, L., Mennella, A., Miville- Deschênes, M. A., Moneti, A., Montier, L., Mora, J., Morgante, G., Morisset, N., Mortlock, D., Munshi, D., Murphy, A., Naselsky, P., Nash, A., Natoli, P., Netterfield, C. B., Novikov, D., Novikov, I., O'Dwyer, I. J., Osborne, S., Pajot, F., Pasian, F., Patanchon, G., Pearson, D., Perdereau, O., Perotto, L., Perrotta, F., Piacentini, F., Piat, M., Plaszczynski, S., Platania, P., Pointecouteau, E., Polenta, G., Ponthieu, N., Poutanen, T., Prézeau, G., Prina, M., Prunet, S., Puget, J. L., Rachen, J. P., Rebolo, R., Reinecke, M., Renault, C., Ricciardi, S., Riller, T., Ristorcelli, I., Rocha, G., Rosset, C., Rubiño-Martín, J. A., Rusholme, B., Sandri, M., Santos, D., Savini, G., Schaefer, B. M., Scott, D., Seiffert, M. D., Shellard, P., Smoot, G. F., Starck, J. L., Stassi, P., Stivoli, F., Stolyarov, V., Stompor, R., Sudiwala, R., Sygnet, J. F., Tauber, J. A., Terenzi, L., Toffolatti, L., Tomasi, M., Torre, J. P., Tristram, M., Tuovinen, J., Valenziano, L., Vibert, L., Vielva, P., Villa, F., Vittorio, N., Wade, L. A., Wandelt, B. D., Watson, C., White, S. D. M., Wilkinson, A., Wilson, P., Yvon, D., Zacchei, A., Zhang, B., and Zonca, A., "Planck early results. II. The thermal performance of Planck," *A&A* **536**, A2 (Dec. 2011).

[3] Dragone, C., "Offset multireflector antennas with perfect pattern symmetry and polarization discrimination," *Bell Labs Technical Journal* **57**(7), 2663–2684 (1978).

[4] Fargant, G., Dubruel, D., Cornut, M., Riti, J.-B., Passvogel, T., De Maagt, P. J., Anderegg, M., and Tauber, J., "Very wide band telescope for Planck using optical and radio frequency techniques," in [*Proc. SPIE Vol. 4013, p. 69-79, UV, Optical, and IR Space Telescopes and Instruments, James B. Breckinridge; Peter Jakobsen; Eds.*], **4013**, 69–79 (July 2000).

[5] Swetz, D. S., Ade, P. A. R., Amiri, M., Appel, J. W., Battistelli, E. S., Burger, B., Chervenak, J., Devlin, M. J., Dicker, S. R., Doriese, W. B., Dünner, R., Essinger-Hileman, T., Fisher, R. P., Fowler, J. W., Halpern, M., Hasselfield, M., Hilton, G. C., Hincks, A. D., Irwin, K. D., Jarosik, N., Kaul, M., Klein, J., Lau, J. M., Limon, M., Marriage, T. A., Marsden, D., Martocci, K., Mauskopf, P., Moseley, H., Netterfield, C. B., Niemack, M. D., Nolta, M. R., Page, L. A., Parker, L., Staggs, S. T., Stryzak, O., Switzer, E. R., Thornton, R., Tucker, C., Wollack, E., and Zhao, Y., "Overview of the Atacama Cosmology Telescope: Receiver, Instrumentation, and Telescope Systems," *ApJS* **194**, 41 (June 2011).

[6] Padin, S., Staniszewski, Z., Keisler, R., Joy, M., Stark, A. A., Ade, P. A. R., Aird, K. A., Benson, B. A., Bleem, L. E., Carlstrom, J. E., Chang, C. L., Crawford, T. M., Crites, A. T., Dobbs, M. A., Halverson, N. W., Heimsath, S., Hills, R. E., Holzapfel, W. L., Lawrie, C., Lee, A. T., Leitch, E. M., Leong, J., Lu, W., Lueker, M., McMahon, J. J., Meyer, S. S., Mohr, J. J., Montroy, T. E., Plagge, T., Pryke, C., Ruhl, J. E., Schaffer, K. K., Shirokoff, E., Spieler, H. G., and Vieira, J. D., "South Pole Telescope optics," *Appl. Opt.* **47**, 4418–4428 (Aug. 2008).

[7] de Bernardis, P., Ade, P. A. R., Baselmans, J. J. A., Battistelli, E. S., Benoit, A., Bersanelli, M., Bideaud, A., Calvo, M., Casas, F. J., Castellano, M. G., Catalano, A., Charles, I., Colantoni, I., Columbro, F., Coppolecchia, A., Crook, M., D'Alessandro, G., De Petris, M., Delabrouille, J., Doyle, S., Franceschet, C., Gomez, A., Goupy, J., Hanany, S., Hills, M., Lamagna, L., Macias-Perez, J., Maffei, B., Martin, S., Martinez-Gonzalez, E., Masi, S., McCarthy, D., Mennella, A., Monfardini, A., Noviello, F., Paiella, A., Piacentini, F., Piat, M., Pisano, G., Signorelli, G., Tan, C. Y., Tartari, A., Trappe, N., Triqueneaux, S., Tucker, C., Vermeulen, G., Young, K., Zannoni, M., Achúcarro, A., Allison, R., Artall, E., Ashdown, M., Ballardini, M., Banday, A. J., Banerji, R., Bartlett, J., Bartolo, N., Basak, S., Bonaldi, A., Bonato, M., Borrill, J., Bouchet, F., Boulanger, F., Brinckmann, T., Bucher, M., Burigana, C., Buzzelli, A., Cai, Z. Y., Carvalho, C. S., Challinor, A., Chluba, J., Clesse, S., De Gasperis, G., De Zotti, G., Di Valentino, E., Diego, J. M., Errard, J., Feeney, S., Fernandez- Cobos, R., Finelli, F., Forastieri, F., Galli, S., Génova-Santos, R., Gerbino, M., Gonzá lez-Nuevo, J., Hagstotz, S., Greenslade, J., Handley, W., Hernández-Monteagudo, C., Hervias- Caimapo, C., Hivon, E., Kiiveri, K., Kisner, T., Kitching, T., Kunz, M., Kurki-Suonio, H., Lasenby, A., Lattanzi, M., Lesgourgues, J., Lewis, A., Liguori, M., Lindholm, V., Luzzi, G., Martins, C. J. A. P., Matarrese, S., Melchiorri, A., Melin, J. B., Molinari, D., Natoli, P., Negrello, M., Notari, A., Paoletti, D., Patanchon, G., Polastri, L., Polenta, G., Pollo, A., Poulin, V., Quartin, M., Remazeilles, M., Roman, M., Rubiño-Martín, J. A., Salvati, L., Tomasi, M., Tramonte, D., Trombetti, T., Väliviita, J., Van

de Weyjgaert, R., van Tent, B., Vennin, V., Vielva, P., and Vittorio, N., "Exploring cosmic origins with CORE: The instrument," *Journal of Cosmology and Astro-Particle Physics* **2018**, 015 (Apr. 2018).

[8] Matsumura, T., Akiba, Y., Arnold, K., Borrill, J., Chendra, R., Chinone, Y., Cukierman, A., de Haan, T., Dobbs, M., Dominjon, A., Elleflot, T., Errard, J., Fujino, T., Fuke, H., Goeckner- wald, N., Halverson, N., Harvey, P., Hasegawa, M., Hattori, K., Hattori, M., Hazumi, M., Hill, C., Hilton, G., Holzapfel, W., Hori, Y., Hubmayr, J., Ichiki, K., Inatani, J., Inoue, M., Inoue, Y., Irie, F., Irwin, K., Ishino, H., Ishitsuka, H., Jeong, O., Karatsu, K., Kashima, S., Katayama, N., Kawano, I., Keating, B., Kibayashi, A., Kibe, Y., Kida, Y., Kimura, K., Kimura, N., Kohri, K., Komatsu, E., Kuo, C. L., Kuromiya, S., Kusaka, A., Lee, A., Linder, E., Matsuhara, H., Matsuoka, S., Matsuura, S., Mima, S., Mitsuda, K., Mizukami, K., Morii, H., Morishima, T., Nagai, M., Nagasaki, T., Nagata, R., Nakajima, M., Nakamura, S., Namikawa, T., Naruse, M., Natsume, K., Nishibori, T., Nishijo, K., Nishino, H., Nitta, T., Noda, A., Noguchi, T., Ogawa, H., Oguri, S., Ohta, I. S., Otani, C., Okada, N., Okamoto, A., Okamoto, A., Okamura, T., Rebeiz, G., Richards, P., Sakai, S., Sato, N., Sato, Y., Segawa, Y., Sekiguchi, S., Sekimoto, Y., Sekine, M., Seljak, U., Sherwin, B., Shinozaki, K., Shu, S., Stompor, R., Sugai, H., Sugita, H., Suzuki, T., Suzuki, A., Tajima, O., Takada, S., Takakura, S., Takano, K., Takei, Y., Tomaru, T., Tomita, N., Turin, P., Utsunomiya, S., Uzawa, Y., Wada, T., Watanabe, H., Westbrook, B., Whitehorn, N., Yamada, Y., Yamasaki, N., Yamashita, T., Yoshida, M., Yoshida, T., and Yotsumoto, Y., "LiteBIRD: Mission Overview and Focal Plane Layout," *Journal of Low Temperature Physics* **184**, 824–831 (Aug. 2016).

[9] Granet, C., "Designing classical Dragonian offset dual-reflector antennas from combinations of prescribed geometric parameters," *IEEE Antennas and Propagation Magazine* **43**, 100–107 (Dec. 2001).

[10] Suzuki, A., Arnold, K., Edwards, J., Engargiola, G., Holzapfel, W., Keating, B., Lee, A. T., Meng, X. F., Myers, M. J., O'Brient, R., Quealy, E., Rebeiz, G., Richards, P. L., Rosen, D., and Siritanasak, P., "Multichroic dual-polarization bolometric detectors for studies of the cosmic microwave background," *Journal of Low Temperature Physics* **176**, 650–656 (Sep 2014).

[11] Suzuki, A., *Multichroic Bolometric Detector Architecture for Cosmic Microwave Background Polarimetry Experiments*, PhD thesis, University of California, Berkeley (Jan. 2013).

[12] Aubin, F., *Detector Readout Electronics for EBEX: A Balloon-borne Cosmic Microwave Background Polarimeter*, PhD thesis, McGill University (2013).

[13] Cuttaia, F., Terenzi, L., Morgante, G., Sandri, M., Villa, F., De Rosa, A., Franceschi, E., Frailis, M., Galeotta, S., Gregorio, A., Delannoy, P., Foley, S., Gandolfo, B., Neto, A., Watson, C., Pajot, F., Bersanelli, M., Butler, R. C., Mandolesi, N., Mennella, A., Tauber, J., and Zacchei, A., "In-flight measurement of Planck telescope emissivity," *ArXiv e-prints* , arXiv:1801.09421 (Jan. 2018).

[14] Richards, P. L., "Bolometers for infrared and millimeter waves," *Journal of Applied Physics* **76**, 1–24 (July 1994).

[15] Mather, J. C., "Bolometer noise: nonequilibrium thoery," *Appl. Opt.* **21**, 1125–1129 (Mar. 1982).